Contents

Summary

This report presents a novel, low cost concept used for solar tracking in equatorial regions around the world. The importance of the inclusion of solar tracking has been established; research into current tracking systems completed and the feasibility of use in different geographical areas has been examined.
Presented is a computer model of the system, a general arrangement design, 3D illustrations and a working prototype. Experimental testing shows considerable agreement with computer models to indicate proof of theory.
The solar tracker is passively activated by aluminium/steel bimetallic strips and controlled by a viscous damper. Computer modelling boast increases in efficiency of up 23% over fixed solar panels.
In addition, scope for further developments to the design are critically evaluated in terms of complexity and benefit.

Glossary

α_{ST}	=	11 x 10^{-6} m/K (Steel)
α_{AL}	=	23 x 10^{-6} m/K (Aluminium)
β	=	Solar altitude (measured from the horizontal East)
C_p	=	Specific heat capacity
C_d	=	Coefficient of Drag
δ	=	Height of boundary layer (taken from ground)
E	=	Composite stiffness
ϕ	=	Angle of Curvature
g	=	Acceleration due to gravity
h	=	Distance of bar mid point to neutral axis
h1, h3	=	Heights of each side of the solar tracker
h2	=	Height of centre axis of rotation
I	=	Composite second moment of area
k	=	Thermal Diffusivity
L	=	Original Length of bimetallic strip (m)
M	=	Mass
μ	=	Coefficient of Friction
ρ	=	Density of respective material
R	=	Radius of Curvature
r	=	Radius of friction moment
$\frac{dT_{AL}}{d\tau}$	=	Rate of change of Temperature w.r.t. Time
ΔT	=	Temperature Change in bimetallic strip (K)
t	=	Thickness of bar
θ	=	Solar tracker angle
u	=	fluid velocity at height y
U_o	=	fluid velocity at boundary layer
V	=	Volume of respective material
x	=	Distance along bimetallic strip
y	=	Height above surface

1. Introduction

There are numerous ways to convert the solar energy into either electricity or heat, be it on an industrial or commercial scale. Although, considering the individual consumer, the two dominant methods are used:

i) Photovoltaic (PV) cells are used to produce electricity
ii) Thermal collection devices to augment central heating systems

Although both sources can benefit from solar tracking, only PV cells will be considered due to the greater need for electricity, rather than hot water, in the developing world.

A standard PV cell is comprises primarily of two layers of crystalline silicon; one negatively doped (with phosphorus) and the other positively doped (with boron). Placing these two layers together, creates an electric field at their junction, i.e. neutrality is disrupted. With the addition of sunlight, free electrons are excited, moving between the layers and further upsetting neutrality. This electron imbalance is converted to a current by providing an external path between the two panels. The electron flow provides a current and the cell's field causes a voltage, and hence power is produced.

This low maintenance, renewable method of electricity production appears to be very useful, however, approximately only 15% of the energy that strikes the panel is converted to electricity[1], and overheating further reduces this value.

2. Using solar tracking to improve solar panel efficiency

A solar tracker strives to force sunlight to contact the PV cell normally at all times throughout the day. Some current devices will change the orientation of the PV cell, but this need not necessarily be the only method. Various sensing equipment and actuating devices, both electrical and mechanical, are in use today.
The presence of a solar tracker is not essential for the operation of a solar panel, but without it, efficiency is reduced. Tests have shown in New Mexico, USA that increases of up to 32% extra power can be produced per annum using a variable elevation solar tracker[2]. It is also reasonable to assume that this figure, now nearly 20 years old, can be increased, given the recent technological advances.

3. The Effect of Geographical Location on Design Factors

Figure 1 shows the various locations around the world for which considerations for solar tracking were made. As solar intensities, temperature and precipitation levels differ throughout the world it is useful to consider some of the options available:

Figure 1: World map of highlighting locations for which factors for solar tracking were considered.

3.1 Brazzaville, Congo-Republic; 4.3^0N, 15.2^0E. As can be seen, this developing world country is close to the equator and hence the altitude angle would consistently be very close to 90^O, hence rendering a dual axis tracker unnecessary. Temperatures in this area would show low variability throughout the year making it easier to design a tracking system that could be effectively used all year.

3.2 Montreal, Canada; 45.5N, 73.6W. This area would experience a different set of challenges to an equatorial location. Summer days would have long periods of daylight, although the temperatures and solar intensities not as great as those at the equator. This would require a tracker to be designed that was able to track for long periods - maximising summer daylight absorption. And conversely, winter days, being very short, would be unable to produce much electricity. Also since the sun, in both summer and winter, is considerably lower in the sky, a single axes system would be inappropriate.

3.3 Nottingham, England; 53.0N, 1.2W. The challenges presented by this area are again different. Other factors such as precipitation would pose more of a maintenance problem and may lower tracking accuracy. Also, cloud cover, even in summer months, would leave a passive tracker unable to accurately locate the sun. In this case an electronic device may be the best solution.

4. Current Technology and its Limitations

Many solutions are currently on the market. The ideal tracker would allow the PV cell to accurately locate the sun, compensating for both changes in the altitude angle of the sun (throughout the day) and latitudinal offset of the sun (during seasonal changes). The slow movement of the sun requires a damped system that will also respond slowly and avoid an oscillatory movement. Other desirable aspects would

include the nocturnal repositioning of the solar tracker to anticipate the alignment of sunrise, opposite to that of the previous day's sunset, reducing lost energy in the morning.

The current technology on market can be categorised as follows:

4.1 Electronic solutions

a) A common solution is that of a centrally pivoted PV cell being moved, about this pivot, by a motor linked to an electronic sensor. This is probably the simplest electronic method available, with the motor being powered by the cell itself. The panel is positioned out of reach, to avoid human interference, although leaving it more susceptible to wind drag. However, as PV power is reduced, this is not a very elegant solution.

b) Another type of electric solar tracker is shown in Figure 2, and includes a sensor that aims to minimise the angle between the line of the sun and a face perpendicular to the panel[3]. When this angle is reduced to zero the sunlight strikes the panel at 90^{O}. Also, in this design, the central pivot was not horizontal – one bearing was nearer the ground than the other – giving the correct elevation for non-equatorial locations. Again the panel itself produced the power for the motor.

Figure 2: An electric solar tracker including a sensor that aims to minimise the angle between the line of the sun and a face perpendicular to the panel.

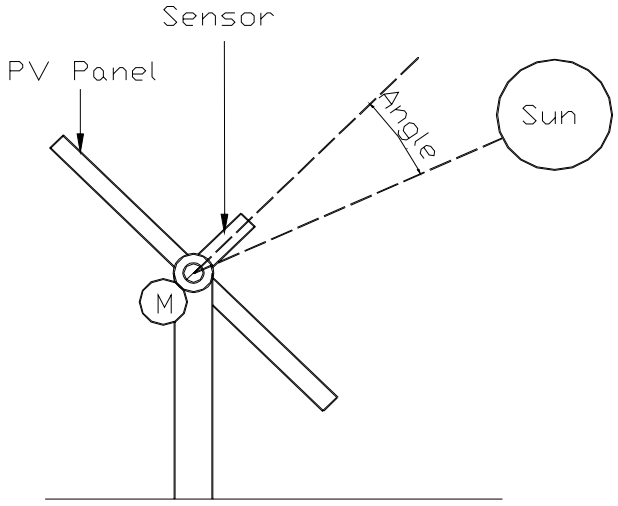

It can be seen that electronic solutions exist, and in fact command the lion's share of the market, but they deplete the power produced by the PV panel for its own operation, and also have the added expense of fitting and maintaining an electric motor and control system.

4.2 Passive solutions

Zomeworks Ltd.[4] supplies a passive solar tracker.

Figure **3** shows how movement is instigated using two identical cylindrical tubes (each at either side of the panel and equal distances from the central pivot) filled with a fluid under partial pressure. Using suitably placed shades, the sun heats the fluid causing evaporation and transfer from one cylinder to the other. This mass imbalance

is used to move the solar panel. Damping is used to limit the speed of movement. This simple system can be cheaply made and uses none of the PV cell's power, although it starts every day pointing in the wrong direction, losing sight of the sun as it attempts to reposition itself. Despite this draw back, it is a commonly used method.

Figure 3: Zomeworks passive solar tracker using two identical cylindrical tubes filled with a fluid under partial pressure.

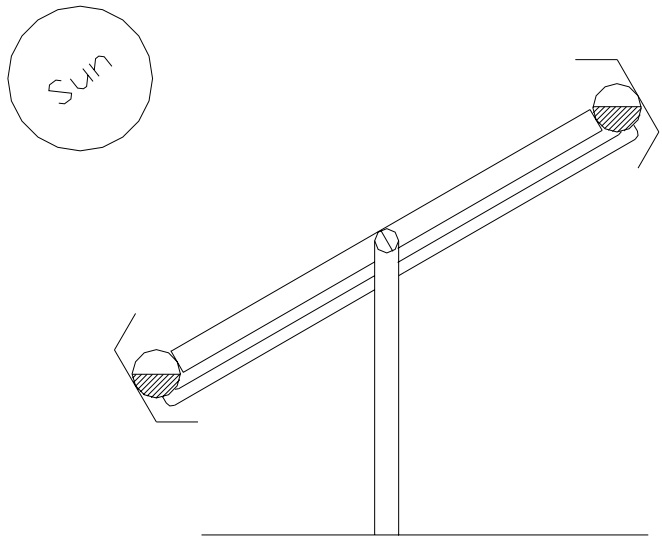

Tests have shown that passive trackers have been found to be comparable to electrically based systems in terms of performance[5], and even though they are less expensive, they have not yet been widely accepted by the consumer.

5. Future Technological Development

For a developing country with limited material availabilities and manufacturing techniques, a simple solution is thought to be best. Also, in order to make the tracker replicable and maintainable, it is thought a passive system should be designed.

Several new concepts have been considered:

5.1 Redesigned passive dual cylinder tracker, using a partially pressurised fluid. This system will effectively compare the temperature between two points.

This tracker has flaws that must be changed if it were to be considered for a developing country. A system of quick return would be useful addition – one-way dampers, springs and eccentrically placed masses have been considered but no appropriate solution has, as yet, been found. It may also be difficult to locate a suitable fluid in the developing world and harder still to pressurise it, inject it into a container and seal it.

5.2 Expanding fluid in a piston (e.g. Automatic greenhouse window opener)

A piston based system that exploits an expansion due to the change of state from solid into liquid when heated similar to that used to open greenhouse windows[6]. This system is heat sensitive and although displacements are small,

the forces generated are large. Again the temperature between two pistons would be compared leaving a resultant force in one direction (as one piston heats up, the other cools down). A problem here would be that the isolation of the fluid from any impurities would be both difficult and expensive, leading to a loss of fluid over time.

5.3 Expanding air in a piston e.g. Sterling engine

This idea involved trapping air in a container on the 'in-stroke', allowing the sun to heat the air, and the piston doing work on the 'out-stroke'. This has the advantage of no fluid to be pressurised during set-up or lost during service. The sealing of any pistons used must be an accurate process and may challenge the skills of developing world technology. Again, this would be a differential process between two oppositely placed air containers. Complexities may also arise due to the oscillating forces produced.

5.4 Expanding fluid in a variable sized container

This principle would work in a similar method to Gallileo's thermometer. A flexible container would be situated either side of a centrally pivoted PV cell, and as one container is heated and one is cooled; the air contained inside them would expand and contract respectively. The change in density would lead to an imbalance in buoyancy forces and move the tracker. This would require the fluid to expand to be lighter than air, and condense to be heavier than air. In theory, this idea sounds possible, but finding a suitable fluid with the correct properties and a suitable expanding container proved more difficult than first imagined.

5.5 Shape Memory Alloys (SMA)

SMA's can be deformed at one temperature but when heated/cooled, will return to their original shape, i.e. the alloys appear to have a memory[7]. This sounds like a simple solution – few moving parts and no fluids to contain. However, the main disadvantage is cost. Nickel-titanium alloys will not be easily or cheaply available in a developing country, so this idea will not be suitable.

5.6 Reflection system

Without moving the PV, devices exist that will deflect the direction of the sunlight to strike a plate normally. A current example uses this idea to cook food using the sun (e.g. on a beach where conventional power sources are absent). Although this device does not actually 'track' the sun it may provide a low cost solution to increase solar panel efficiency. However, before this idea would be used with solar panels, a material would have to be found that would reflect visible light wavelengths and not infra-red heat, as this would reduce the effectiveness of the PV cell. As yet no material with this property has been found.

5.7 Expanding metal / bimetallic strip

The physics behind expanding metals indicate that although generated deflections are small, the corresponding forces are large. The bimetallic strip has obvious advantages – the strip will bend in one direction with heat and in the other when cold. Due to the extremely low temperatures in an African night, this provides significant scope for a method of automatic return after the end of the day. This system also boasts the absence of complex fluid

containment and accurate fitting of pistons. It is for these reasons that the bimetallic strip will be used as the trigger for the solar tracker.

6. Solar Tracker Design

The final solar tracker design incorporates two bimetallic strips positioned, on a wooden frame, symmetrically either side of a central horizontal axis. The bimetallic strips are shaded so that the strip furthest from the sun absorbs solar radiation while the strip closest remains shaded and in an isothermal state. As the unshaded bimetallic strip gets hotter, the aluminium heats more than the adjacent steel and, as a result of end and centre constrictions, bending occurs. This bending causes a maximum deflection at the strip midpoint and with the attached mass, an unbalanced moment results throughout the system instigating movement. The solar panel, also held in the frame, is reorientated by this movement towards the sun, ultimately increasing its efficiency.

6.1 Features

Several features, separating this design from others, are present. Some are essential for the correct working of the system while others make it more efficient.

- A feature essential to the correct working of the system included the bimetallic strip bending towards the direction of the sun, meaning that the resulting moment reorientates the solar tracker towards the sun rather than away. This resulted in the heating of the bimetallic strip positioned on the other side of the central axis to the position of the sun.
- The shades had a two-fold effect – reflecting solar radiation away from the shaded bimetallic strip and onto the heated one (thereby increasing its rate of heating).
- The very nature of the design, i.e. two bimetallic strips working against each other, will always attempt to locate the sun, even after the sun emerges from behind a cloud.
- Due to the slow response of the bimetallic strip in respect to other forms of instigation (e.g. partially pressured fluid), the damping of the system also must be greater to control the motion. Consequently the effect of even sporadic, moderate winds will largely be eliminated, as energy absorption will quickly negate their effect.

6.2 Material selection

Material selection was a compromise between two driving factors – the need to obtain the best material for the function of the component over its full life, and the desire to ensure these materials were obtainable in the developing world, cheap, compliant to basic machining processes and maintainable.

- The fixed frame was constructed from timber, although any lightweight wood could be used. It may be desirable to change the form of this base depending on method of mounting. If the base is to be driven into the ground, a stiffer, stronger material may wish to be considered.
- The moveable frame from holding the solar cells and tracking controls were also constructed from timber. Again this was chosen on both structural and economic grounds. Its high specific stiffness, is beneficial to the tracker operation and it ease of fabrication and acquisition make it an attractive choice.
- The materials used for the bimetallic strips were a crucial choice. These materials, as well as satisfying the practical difficulties of acquisition, also needed to boast mechanical properties congruent those in a bimetallic strip:

- Sufficient difference in thermal expansivities facilitated the temperature, and hence stress, differential to be set up and a bending moment to result.
- A high yield stress, allowed large bending deflections without permanent strain.
- With continuous heating and cooling, therefore tensile stressing and relaxation, the fatigue resistance of the material is vital element in the prolonging of the life of the overall life.
- The resistance of the material to creep relaxation during use was essential. Stress relaxation would cause the strain differential generated during heating to be dissipated, reducing the resultant bending moment. However, providing the temperature of the bimetallic strip is less than 30% of the material melting point, creep failure is not a problem[8].
- Material stiffness will dictate flexural rigidity of the bimetallic strip. This is a comprise between a desire for bending during heating and an aversion from it in the absence of solar radiation.

Considering all of the above factors, a steel-aluminium composite bar was chosen for its ease of manufacture, acquisition, and suitable thermal and mechanical properties.

- Criteria for the remainder of material selection decisions were a balance between ease of acquisition, low cost, lightweight and reasonable mechanical properties.

7. C Program Solar Tracker Model

7.1 General System

At the design stage, a C computer program was complied as an aid to visualisation of solar tracker operation. Each stage of the system from solar heating to reorientation of the solar panel towards its optimum position is incorporated. This program is shown in Appendix 2. The system can be broken down different phases as shown on the flow chart in Figure 4.

Figure 4: Flow chart describing the processes undertaken in the solar tracker

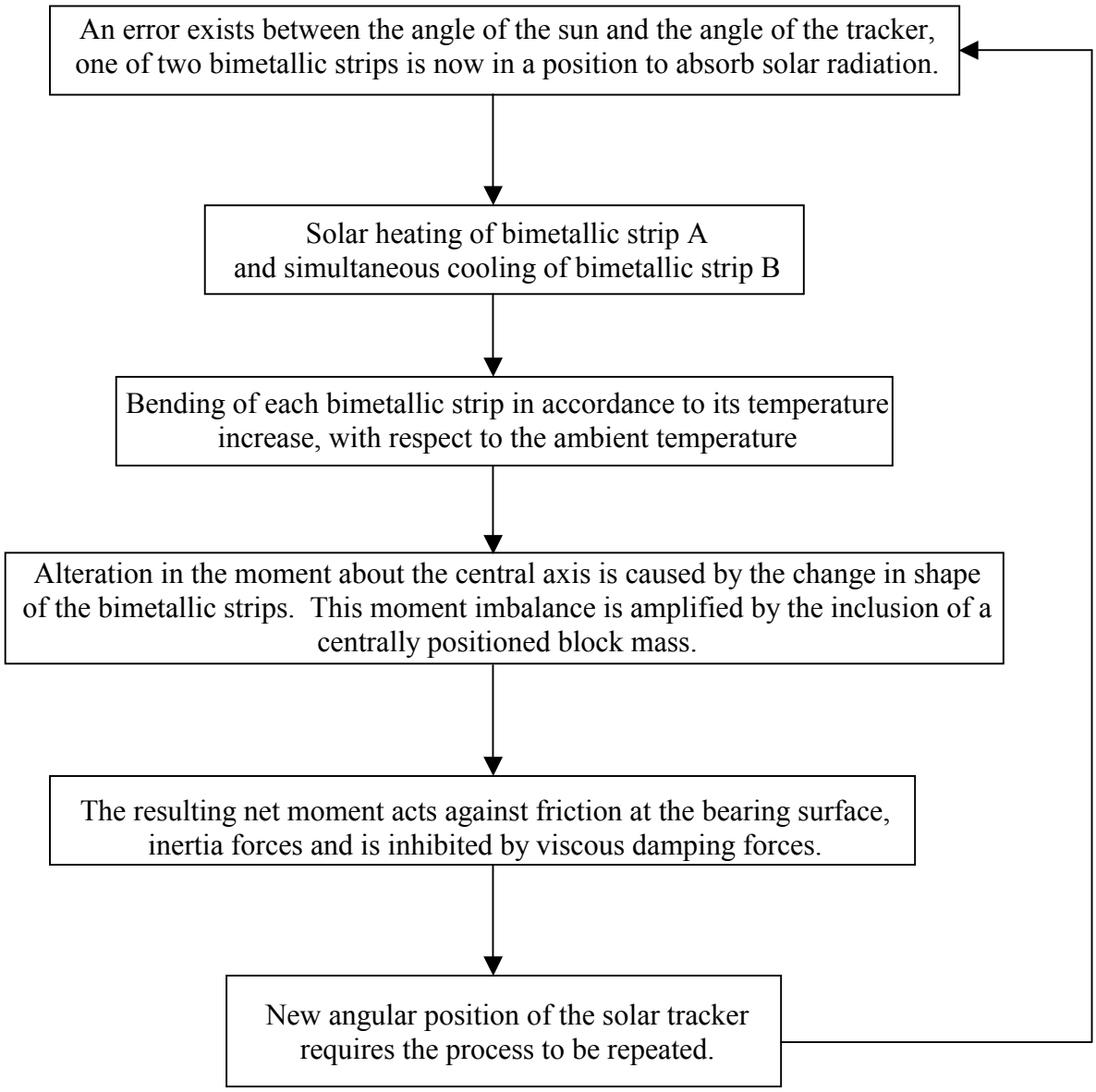

The outlined stages are now described in more detail:

7.2 Thermodynamics

The thermodynamic effects on a solar tracker are two simultaneous heating processes. The presence of an error in the tracker angle from that of the sun, will subject one bimetallic strip to solar radiation, while the other is receiving no

radiation in the shade. In an environment heated by solar radiation, a material attempts to reach an equilibrium temperature where the energy sources arriving at the material equal energy sinks leaving it[9], i.e.

Solar Radiation = Radiation losses + Convection losses

However, until the material reaches this equilibrium, the difference in energy is conducted through the bar.

Conduction = Solar Radiation - Total Losses

As the temperature of the bar increases, the losses become greater and hence the rate of energy conduction decreases i.e. unsteady heat conduction. However, if the bar is sufficiently thin this complex model can be simplified to a lumped mass system where it is assumed that the material heats up equally across its thickness. A proof of the accuracy of this assumption is given in Appendix 1.

This allows a model for heat conduction through the bar to be written as:

Equation 1: $$\sum Q = m.c_p.\frac{dT_{AL}}{d\tau}$$

Where:

M = Mass

C_p = Specific heat capacity

$\frac{dT_{AL}}{d\tau}$ = Rate of change of Temperature w.r.t. time

Therefore, from Equation 1,

Equation 2: $$Q_{SOLAR} - Q_{LOSSES} = m.c_p.\frac{dT_{AL}}{d\tau}$$

Rearranging Equation 2, and stepping over small increments of time, a change in temperature of the bar is found:

Equation 3: $$\Delta T_{AL} = \frac{\sum Q.\Delta\tau}{mc_p}$$

The resulting increase in temperature can be used to model the bending of this composite bar.

7.3 Beam Bending

Using this result for stepped temperature increase, the subsequent bending for both bimetallic strips can be found.
The deflection of the bar is calculated in two stages:
i) The deflection is found for a given temperature increase, free of external loading and hence, the resulting bending moment, due to heating alone, is found.
ii) Onto this bending moment, are imposed other applied forces like the self-weight of the bar and the block masses.

i) The deflection due to a temperature increase is found as follows:
The thermal strains can be calculated using the coefficients of thermal expansion, α, for both materials[10]:

Equation 4: $\varepsilon_{Thermal} = \alpha_{Material}.L.\Delta T$

Where α, for the two materials are
α_{ST} = 11×10^{-6} m/K
α_{AL} = 23×10^{-6} m/K
L = Original Length (m)
ΔT = Temperature Change (K) from Equation 3

Assuming the bimetallic strip's bending shape is in the arc of a circle, the following statements apply:

Equation 5: $L_{ST} + L.\varepsilon_{ST} = R_{ST}.\phi$

Equation 6: $L_{AL} + L.\varepsilon_{AL} = R_{AL}.\phi$

Where:
R = Radius of Curvature
ϕ = Angle of Curvature

But since the angle of curvature, ϕ, is the same for both materials, then Equation 5 and Equation 6 can be combined to give:

Equation 7: $$\frac{L_{AL} + L_{AL}.\varepsilon_{AL}}{R_{AL}} = \frac{L_{ST} + L_{ST}.\varepsilon_{ST}}{R_{ST}}$$

And using geometry:

Equation 8: $$R_{AL} = R_{ST} + \left(\frac{t_{AL} + t_{ST}}{2}\right)$$

Where:
t = Thickness of bar

Combining Equation 7 and Equation 8, the following expression for radius of curvature can be found:

Equation 9: $$R_{ST} = \left(\frac{L_{ST} + L_{ST}.\varepsilon_{ST}}{L_{AL}.\varepsilon_{AL} - L_{ST}.\varepsilon_{ST}}\right) \times \left(\frac{t_{AL} + t_{ST}}{2}\right)$$

The angle of curvature, ϕ, can now be found

Equation 10: $$\phi = \frac{L_{AL} + \varepsilon_{AL} L_{AL}}{R_{AL}}$$

However, the bending moment on a bimetallic strip cannot be assumed to be equivalent to a simple applied load, without one other consideration – the shifted

neutral axis. The neutral axis, i.e. the line that remains the same length irrespective of the degree of applied bending, is necessary to accurately model the flexural rigidity provided by each bar in the bimetallic strip. Using the result in Equation 10, the radius of the neutral axis of bending is found by:

Equation 11: $R_{NEUTRAL} = \frac{\text{Unstrained Length}}{\phi}$

Hence, the second moment of area for each bar can be calculated:

Equation 12: $I_{AL} = \frac{bd^3}{12} + Ah^2$

Where:
h = Distance of bar mid point to neutral axis

It is notable that the midpoints of both aluminium and steel, are located on the tensile side of the neutral axis. This is consistent with prior analysis as both bars are expanding with increasing temperature.
Using the above equations, the applied moment, M_o, on the bar due to thermal effects is found using simple beam bending equations:

Equation 13: $M_o = \frac{EI}{R}$

Where:
R = Average of the two radii of curvature
E = Stiffness
I = Second moment of area found from Equation 12

ii) The second stage involves finding the total deflection considering the other forces present. Figure 5 shows the different forces acting on the bar.

Figure 5: All forces acting on the bimetallic strip

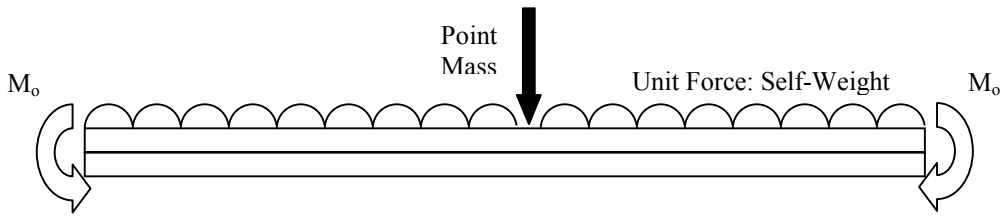

The other forces present include:

- Self-weight of the bar. This is modelled as uniformly distributed load across the length of the beam and varies as the solar tracker re-orientates itself throughout the

day. The effect of the moment rises to a peak in the centre of the bar and is given by Equation 14:

Equation 14: $M_{WEIGHT} = \frac{1}{4} x^2 . g . \cos\theta . (V_{AL}\rho_{AL} + V_{ST}\rho_{ST})$

Where

x	=	Distance along bimetallic strip
g	=	Acceleration due to gravity
θ	=	Solar tracker angle
V	=	Volume of respective material
ρ	=	Density of respective material

- Moment of block mass. The steel blocks are positioned at the midpoint of the bimetallic strip and are assumed to act as a point load. The bending moment again rises to a peak in the centre of the bar and varies with the angle of the solar tracker. The moment is given by Equation 15:

Equation 15: $M_{POINT} = \frac{1}{4} x . \cos\theta . g . V_{BLOCK}\rho_{BLOCK}$

Summing the moments calculated in at stepped intervals along the bar. The net moment applied is found by summing Equation 13, Equation 14 and Equation 15:

Equation 16: $\text{Net moment} = M_{THERMAL} + M_{WEIGHT} + M_{POINT}$

By considering the deflection of the beam under this irregular compilation of moments as a boundary value problem, a finite difference method can be incorporated into the computer program.
Splitting the beam into many small steps, the second derivative of y with respect to x (i.e. the rate of change of slope) is given by:

Equation 17: $\frac{d^2y}{dx^2} = \frac{y_{i-1} - 2y_i + y_{i+1}}{\Delta x^2}$

And using the standardised equation for bending moment:

Equation 18: $\frac{d^2y}{dx^2} = -\frac{M(x)}{EI(x)} = -C(x)$

A value for the deflection at any point along the beam is established:

Equation 19: $y_i = \frac{1}{2}\left(\Delta x^2 C(x_i) + y_{i+1} + y_{i-1}\right)$

7.4 System Orientation

The torque about the central axis of rotation is now unbalanced. This torque, provided by each bimetallic strip is:

Equation 20: $\text{Torque} = g . V_{BLOCK}\rho_{BLOCK} Y_{MAX}$

Inhibiting this movement is friction at the pivot:

Equation 21: Friction = $gM\mu r$

μ	=	Coefficient of Friction
M	=	Total Moveable of Mass
r	=	Radius of friction moment

When starting from stationary, the torque resulting from the difference in deflections from each bimetallic strip produce the instigation for movement, and hence reorientation, must over come the friction of the pivot. This is found by combining Equation 20 and Equation 21:

Equation 22:

Net torque =

Torque $_{BMS\,1}$ - Torque $_{BMS\,2}$ – Friction – (Inertia x $\overset{**}{\theta}_i$) – (Damping x $\overset{*}{\theta}_i$)

Although initial values of angular velocity and acceleration are zero, values during following time steps are not. Using this value for net torque, the angular acceleration can be calculated by considering the total inertia of the system about its central pivot:
Angular Acceleration,

Equation 23: $$\overset{**}{\theta} = \frac{\text{Net Torque}}{\text{Inertia}}$$

Hence, values for angular velocity and, ultimately, angular displacement of the solar tracker can be found. The value for angular velocity is dependent on both the previous velocity and the effect of acceleration over the previous time period:

Equation 24: $$\overset{*}{\theta}_i = \overset{*}{\theta}_{i-1} + \tfrac{1}{2}\left(\overset{**}{\theta}_i + \overset{**}{\theta}_{i-1}\right)\Delta\tau$$

In a similar way, the angular displacement can be found by considering the effect both the velocity and acceleration have had on the previous value of displacement.

Equation 25: $$\theta_i = \theta_{i-1} + \tfrac{1}{2}(\overset{*}{\theta}_i - \overset{*}{\theta}_{i-1})\Delta\tau + \tfrac{1}{2}(\overset{**}{\theta}_i - \overset{**}{\theta}_{i-1})(\Delta\tau)^2$$

7.5 Efficiency

Efficiency is defined as the ratio of power output to incident radiation. The power obtained by the solar tracker is assumed to be inversely proportional to the obliquity factor[11], i.e. the cosine of the error angle between the sun and the solar panel. Obviously as this angle increases, the power obtained, and hence the efficiency, of the solar panel is reduced. Beyond an angle of 90°, solar radiation no longer has any direct contact on the solar panel and hence no energy conversion occurs. For the model in question, in order to find the efficiency, some factors have to be noted:

- The solar tracker is only able to follow the sun up to 60^o either side of vertical.
- The solar intensity varies throughout the course of a day. It is modelled by an approximation given by Robinson (1964)[12], and shown in Equation 26:

Equation 26: Solar Intensity = $1200\sin\beta$ W/m^2

Where
β = Solar altitude (measured from the horizontal East)

- The ambient temperature also increased to a peak throughout the day. This temperature rise is modelled by and was derived from known initial boundary conditions:

Equation 27: Ambient Temperature = $19.2\sin(\beta) + 278.9$ Kelvins

These variables dictate the theoretical attainable efficiency, and changing these variables for different locations would also alter the maximum possible efficiency. Three different levels of daily power obtained were calculated. These levels allow for the calculation of two efficiency increases – a theoretical optimum (for the specified conditions) and an actual efficiency produced by the solar tracker.
First, it is necessary to find the power obtained by a stationary horizontal solar panel as this gives an accurate gauge of increases due to any tracking system. This is found as follows:

Equation 28: $\text{Power}_{\text{FIXED}} = \sum(\text{Solar Radiation}/\Delta\tau)\times\cos(\beta-\theta)\times\Delta\tau$

But since the angle of the solar panel, θ, is fixed at 90^o, i.e. fixed horizontally, this can be simplified to:

Equation 29:
$$\text{Power}_{\text{FIXED}} = \sum(\text{Solar Radiation}/\Delta\tau)\times\cos(\beta-\frac{\pi}{2})\times\Delta\tau$$
$$= \sum(\text{Solar Radiation}/\Delta\tau)\times sin(\beta)\times\Delta\tau$$

This value can now be used as a base value against which others can be measured. The power output of the solar panel when mounted on the designed solar tracker is found in a similar way. However, in this case the angle of the solar panel, θ, varies with the tracker response throughout the day, and can, over small time steps, be described using Equation 30:

Equation 30:
$\text{Power}_{\text{TRACKED}} = \sum(\text{Solar Radiation}/\Delta\tau)\times\cos(\beta-\theta)\times\Delta\tau$

However, if the absolute angle $|\beta-\theta|$ is greater than 90^o, the solar panel will receive no direct solar radiation and 0W/m^2 is noted for that time period. Although this decreases efficiency, this occurrence is most common in the earlier morning while the solar tracker is still pointing in the opposite direction from the previous evening. The power output from the sun in the early morning is much lower than at midday, say, and so the reduction in efficiency is not as great as first thought. These efficiencies will be used to quantify that loss.

The third level of obtained power, will be that of the perfect solar tracker. This occurs when the angle between the solar panel and the sun, i.e. the error, is zero at all points throughout the day. A value for this is described as follows:

Equation 31: $$\text{Power}_{\text{OPTIMAL}} = \sum(\text{Solar Radiation}/\Delta\tau)\times\Delta\tau$$

By considering how much better the tracked power output is from the stationary panel output, the efficiency of the solar tracker can be calculated from Equation 29 and Equation 30:

Equation 32: $$\text{Extra Efficiency}_{\text{TRACKER}} = \frac{\text{Power}_{\text{TRACKED}}}{\text{Power}_{\text{FIXED}}}$$

This value can be compared to the optimum efficiency, i.e. how much extra power the perfect solar tracker is capable of obtaining, found by considering Equation 29 and Equation 31:

Equation 33: $$\text{Extra Efficiency}_{\text{OPTIMUM}} = \frac{\text{Power}_{\text{OPTIMUM}}}{\text{Power}_{\text{FIXED}}}$$

These extra efficiency calculations can be used to test the impact of a number of key factors controlling the efficient operation of the solar tracker. They will now be explored.

7.6 Tracker sensitivity

7.6.1 Bimetallic Strip Dimensions

Ultimately the dimensions of the bimetallic strips will dictate the amount of bending at different temperatures over different time periods. All beam dimensions, although especially bar thickness, must reach a compromise to satisfy as many requirements as possible – Reduction in bar thickness will allow increased heat exchange, and hence bending, which accelerates the responsiveness of the solar tracker. However, thinner strips will also cause a larger undesirable deflection under the point mass, thereby increasing the early morning ‘wake up’ response time.

Figure 6 shows thinner bimetallic strips will also be more likely to reach yield stress at its surface and have a lower fatigue resistance.

Figure 6: Bending Stress variations of heated bimetallic strips of different thickness

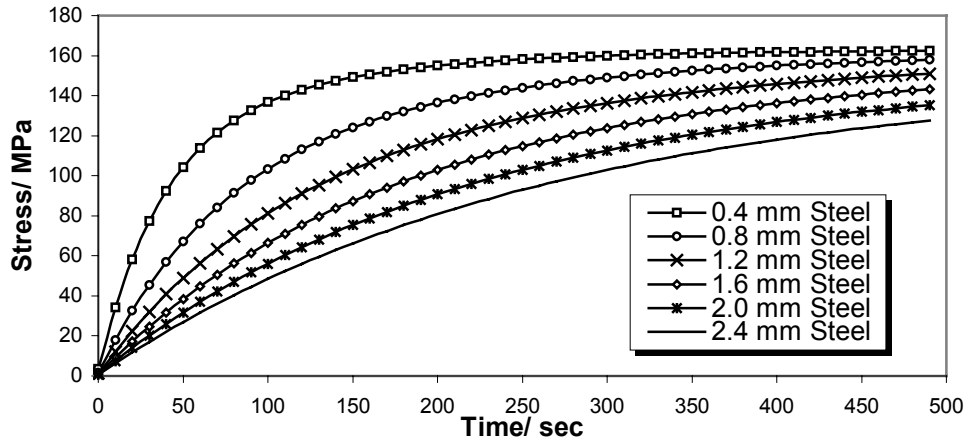

7.6.2 Damping Effects

In a system where two opposing means of movement are constantly working against one another, a level of damping is required. However, if damping is not applied in the correct measures, the system will continually oscillate or be too sluggish to respond.

In order to maximise the efficiency of the solar panel, the damping required must be linked to the rate of response of the system, i.e. the bimetallic strips. As the flexural rigidity of the bimetallic strip increases, i.e. its willingness to bend decreases, and the level of system damping must rise to slow any movement long enough for the slower system to react. Figure 7, produced from the computer model of the system, shows how the efficiency of the solar tracker changes as the level of system damping increases. It can be seen that for an under damped system, excess oscillations actually decrease solar efficiency. It is not until a critical level of damping has been reached that the solar tracker is able to properly function. Effectively, the heavy levels of damping are necessary to inhibited tracker movement before the bimetallic strips have had time to react.

Figure 7: Graph showing the increase in efficiency compared to a fixed solar panel, with increasing levels of damping.

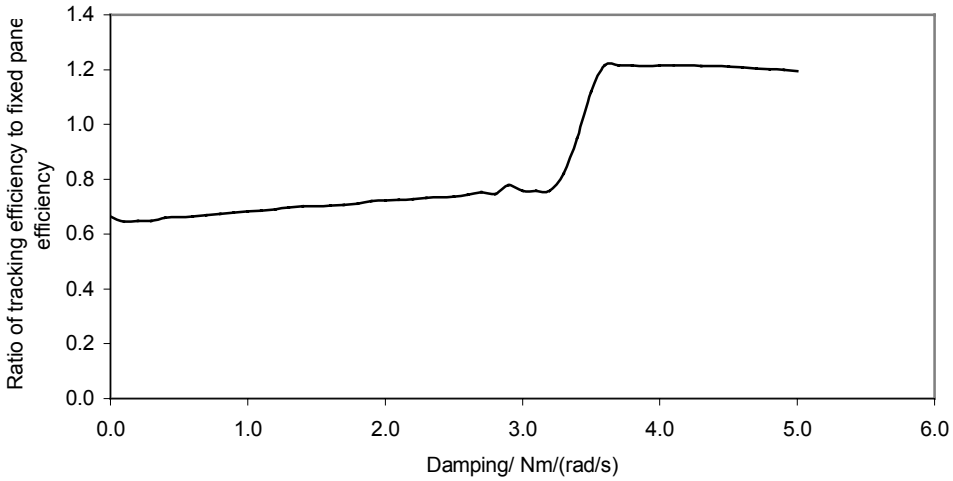

7.6.3 External Disturbances

Tracking the sun in an ideal scenario would involve nothing to alter either the system inputs or outputs. However, when put into practice, factors may contrive to ensure either solar radiation does not reach the solar tracker (e.g. clouds) or an additional external force moves the tracker from its optimum position (e.g. wind, human interference). In either case it is important for the solar tracker to be able to 'find' the sun at any point in the sky, any time throughout the day. Again, system responsiveness (bimetallic strip materials and dimensions) and system damping both contribute to the solar tracker's ability to readapt after a disturbance.
Three disturbances will be considered:

- Wind

The drag over the solar tracker comprises of two main forms:
- Friction drag is present when the panels are close to horizontal.
- Pressure drag is prominent when the tracker is positioned closer to vertical.

As an initial model, the coefficient of drag is modelled as a flat plate, the area of which varies with tracker angle, θ. The seventh power law, as shown in Equation 34, can approximate the air velocity over the tracker[13]:

Equation 34: $$\frac{u}{U_o} = \left(\frac{y}{\delta}\right)^{1/7}$$

Where

u	=	fluid velocity at height y
Uo	=	fluid velocity at boundary layer
y	=	Height above surface
δ	=	Height of boundary layer (taken from ground)

Taking small changes,

Equation 35: $$du = \frac{U_o}{\delta^{1/7}}(dy)^{1/7}$$

For a known velocity at any height above the ground the drag on a tilted plate can be found:

Equation 36: $$\text{Drag} = \tfrac{1}{2} C_d \rho A U^2$$

Using Equation 35 and Equation 36, wind drag must be integrated over the area of the tilted solar tracker. Equation 37 shows the resulting moment:

Equation 37: $$dM = \tfrac{1}{2} C_d \rho A \cos\theta \left(\frac{U_o}{\delta^{1/7}}\right)^2 \left[\left(\int_{h_2}^{h_1} (y-h_2)^{7/2}.dy\right)^{1/7} - \left(\int_{h_3}^{h_2} (h_2-y)^{7/2}.dy\right)^{1/7}\right]^2$$

Where

h1, h3	=	Heights of each side of the solar tracker
h2	=	Height of centre axis of rotation

This moment differential about the central axis, due to the effect of wind, can be incorporated into the computer model as a continual force or in sporadic burst.
As expected, in the case of sporadic impulses the effects of wind are least pronounced with higher damping values. The high levels of system damping facilitate the dissipation of wind energy.
However, with a constantly forcing wind, it was necessary to examine two cases:

i) Wind that inhibited motion in the tracking direction produced a lag in the tracking accuracy. This indicated that accuracy would improve if damping were reduced.
However,

ii) Wind that enhanced the solar tracker's desire to rotate towards the west produced the opposite problem. System accuracy would have been improved had damping been increased.

Improbable as either situation is, it is obviously impossible to satisfy both, and a balance between he two must be sought. It can be assumed that the original value of damping used was satisfactory.

- Partial absence of solar radiation

In the case of a cloud temporarily blocking the radiation getting to the solar tracker, the position will not immediately change. Since the system is balanced about its central pivot, the temperature of both bimetallic strips will decrease towards ambient temperature. With the absence of any applied moment from the effect of heated bimetallic strips acting, the system will slow. However, the moment due to the effect of gravity on point masses may remain, continuing to enforce a 'residual' net moment about the pivot.
In this case, again, a balance must be sought with the level of damping applied. Although, heavy damping will inhibit any residual movement, keeping the tracker in a similar position for when the sun is again visible, light damping will reduce the adjustment time needed to refocus on the sun.

In general with any external disturbance, a quick realignment with the sun is desirable (and obtained by reducing levels of damping), however, to avoid excess oscillatory movement during normal operation, levels of damping must also be sufficiently high. Hence for each solar tracker design, assigning a value of system damping to satisfy both objectives as far as possible, is fundamental to the accuracy of the overall system.

8. Solar Tracker Manufacture

8.1 Method of manufacture

Due to material selection, the methods of manufacture used are all basic processes. However, several dimensions have tolerances below 0.1mm error.

Bearings turned on a lathe, the close tolerance allows for free movement but restricts the size of external asperities from becoming lodged in the bearing. A high standard of surface finish is also achievable on a lathe, reducing friction on the bearing.

8.2 Alterations

Throughout the manufacture, it became evident that the choice of available materials, although substantial, was not exclusive. Some design alterations had to be made and although minor, merit a mention at this stage:

- A 'C' channel section was to be used for pivot connections on both the bimetallic strips and the adjacent fixed pivot. This system would allow freedom of movement for the bar in bending towards and away from the pivot but would restrict it bending in any other direction.
  However, as the specified parts were unavailable, a suitable substitute was designed using an angled section instead of the previous 'C' channel. The drawback with this was the tendency to topple without a constraint. This is illustrated in Figure 8, showing both old and new designs.

Figure 8: Showing old and new pivot 'C' channel sections

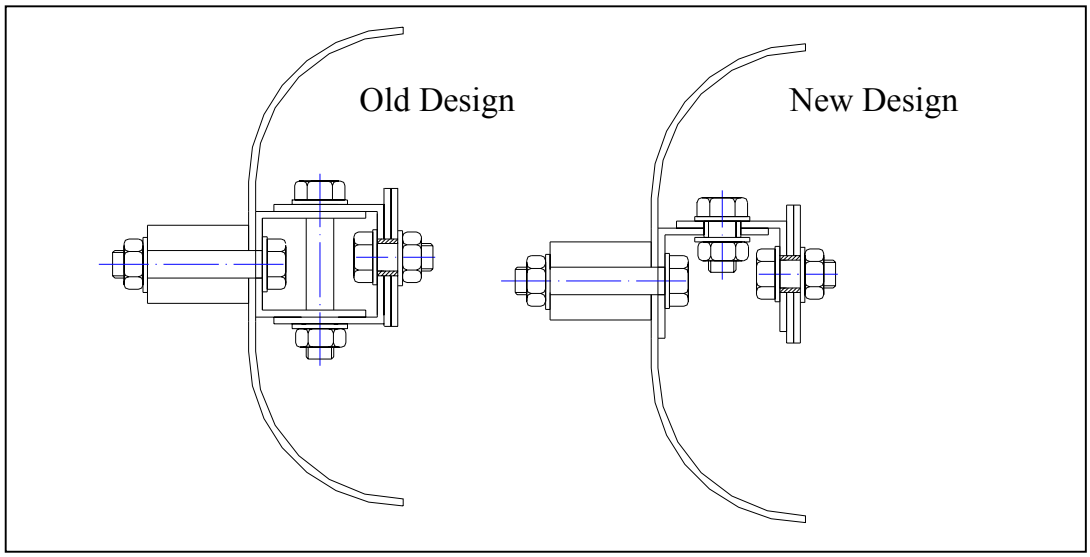

- To avoid losing any thermal strain to loose fitting, a sleeve was designed to fit over the M12 bolts holding the aluminium and steel bars together. This sleeve was designed with a interference fit, shaft basis tolerance on its outer diameter and was tapped internally to an M12 thread allowing the bolt to fasten in position. Figure 9 shows the assemblies after the alteration.

Figure 9: Illustrates additional sleeve used to reduce strain losses in the bolt

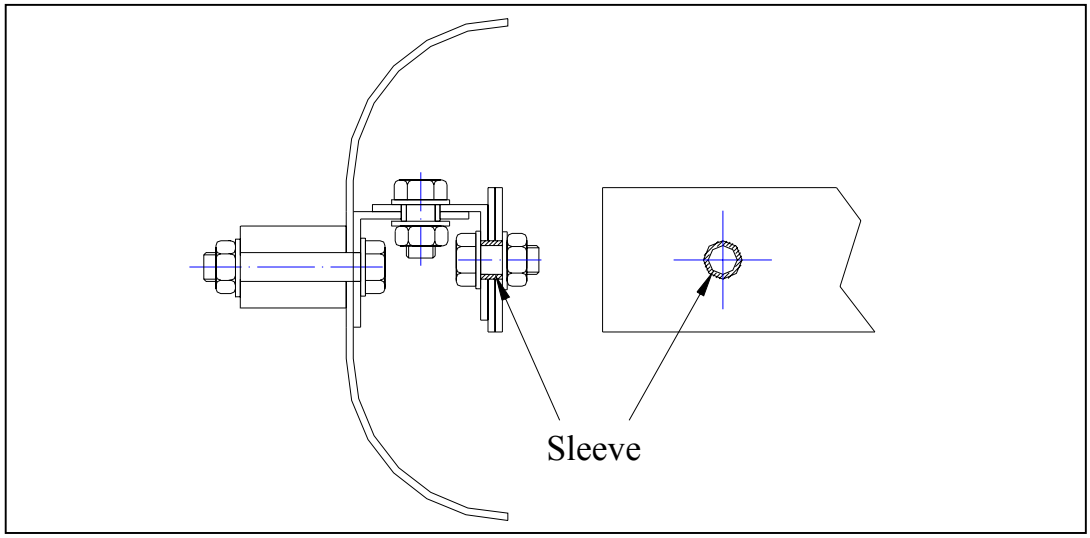

The completed prototype is shown in Figure 10.

Figure 10: Completed solar tracker prototype

9. Solar Tracker Testing

9.1 Bimetallic strip testing

In order to confirm the validity of the proposed theory, it was necessary to compare tested results with numerical predictions. Initial testing of the bimetallic strips used two different material combinations. This testing effectively measured the maximum deflections from a vertical cantilevered position. Although, bars were bonded too thick, results were still in general agreement.

Testing was conducted again after the thickness of the bimetallic strips had been revised. The tests were carried out horizontally whilst attached to the solar tracker, and hence constrained by pivots at each side. Mid point deflection was measured. Setting the solar tracker at a horizontal, one bimetallic strip was heated under known conditions. This removed the self-weight of the bimetallic strip and the point load from deflection equations, testing only the bending caused by heating. The testing was set-up as shown in Figure 11:

Figure 11: Set-up for bimetallic strip testing

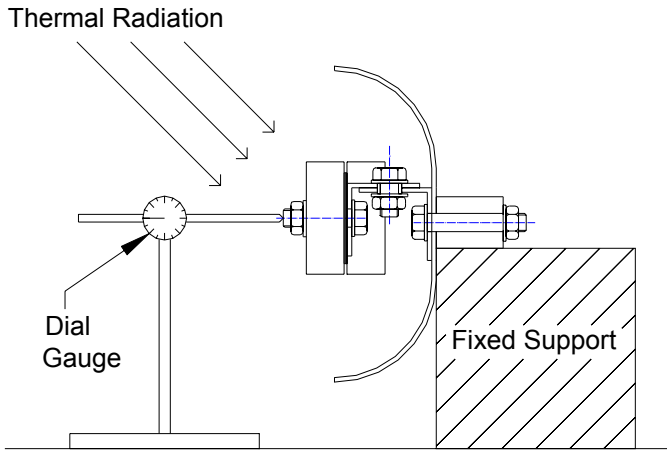

Values of maximum deflection (midpoint of beam) were noted at regular time intervals. Experimental conditions were noted and included in the computer model:

- Thermal radiation level was measured using a pyronometer and voltmeter.
- Ambient temperature was measured using a thermometer.
- Bimetallic strip temperature was measure using a thermo-couple.

As shown in Figure 12, comparisons the experimental results with the model showed good agreement.

Using the previously proven validity of earlier calculations a second round of testing was carried out during the assembly stages taking into consideration the attached masses on each strip. However these calculations show poor agreement with the modelled results. The bending sought was much less than expected. The reason for this was twofold. The bars each 3.175mm thick, required a substantial bending moment to produce a sizeable deflection. However, it is believed the one

key difference was that these bimetallic strips were held at three discrete points along the bar instead of the previously bonded specimens tested before.
The explanation concerns the elastic-plastic deformation at the stress concentration points at each strip. For a hole in a under a tensile load, an approximate value for the stress concentration factor (SCF), $K_T = 3.0$. Hence shear loading, due to the presence of the temperature differentials, will increase threefold for both metals at the SCF. This stress can be modelled in one of two ways – using the Linear rule (applicable for plane strain conditions) or the Neuber Rule (applicable for plane stress conditions). In this case plane stress can be assumed and hence the resulting shear found.

To overcome this problem a polyester resin, namely Araldite™, was used. This leads to a continuous bond along the length of the bar with no obvious stress concentration factors. The resulting bimetallic strips were retested and the results again show better agreement with the previously designed model. This can be seen

Figure 12, which shows the agreement of experimental testing to the results, produced by the computer program.

Figure 12: Graph illustrating both modelled and actual deflections of the bimetallic strip due to the effects of thermal radiation.

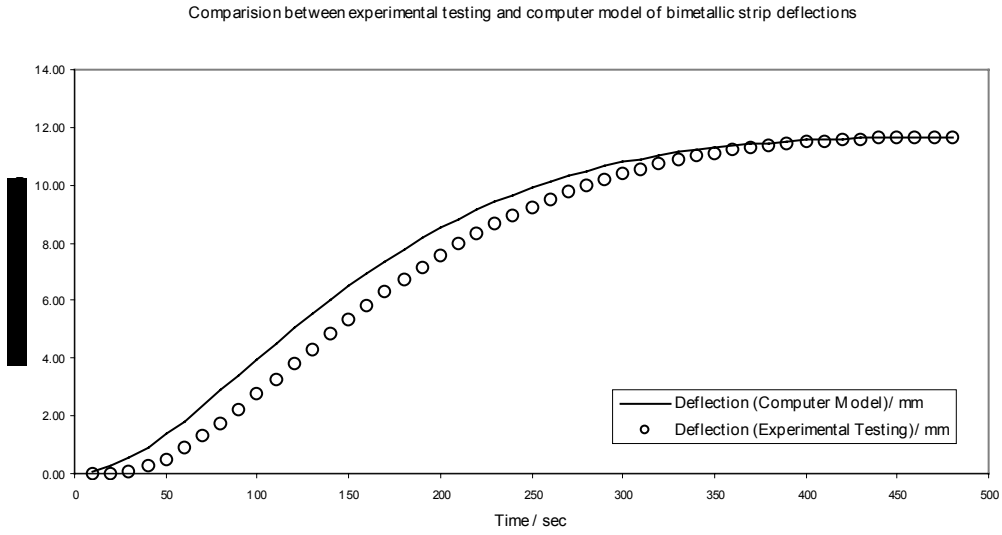

9.2 Dynamic 'Early Morning' Response

The early morning response can be defined as the length of time between the emergence of the sun (i.e. dawn) and the point when the solar tracker has managed to completely reorientate to itself to face the sun. At this time of day the solar tracker must use low, but steadily increasing, values of solar radiation. This means that, although it will take a period of time to correct itself, the lost radiation that would have struck the solar panel in the early morning .
To quantify this problem, several tests can be modelled on both the computer program and using the prototype:

- The time taken until reorientation was measured and compared with the computer model, as shown in Figure 13. It can be seen that as the degree of solar radiation decreases, the time taken to reorientate the tracker grows exponentially, up until the point solar radiation is insufficient to initiate movement.

Figure 13: Showing the time taken for the solar tracker to reorientate from West to East comparing the computer approximations with experimental results

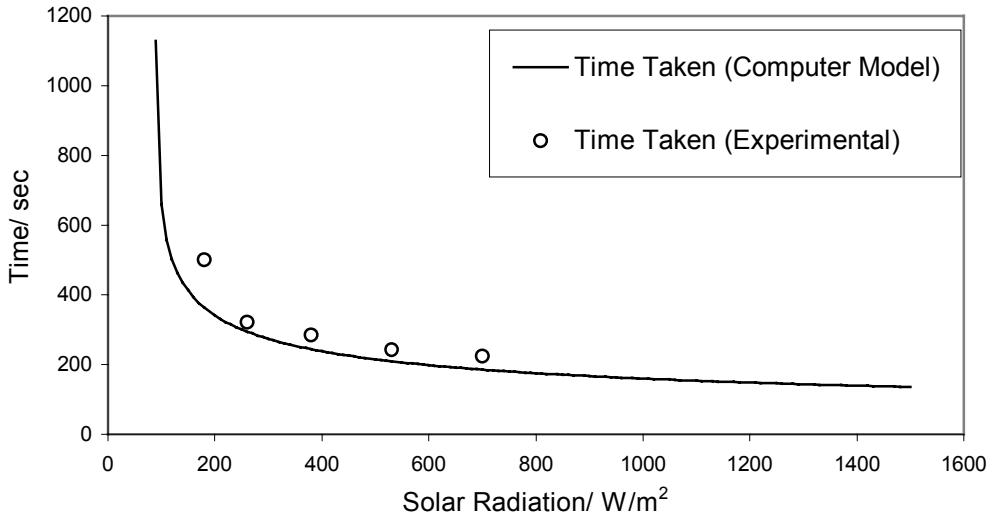

However, since the computer model considers only one set of geographic conditions, a general estimation for the percentage of unexploited power must be found by other means.

- A better illustration of the effect of response times on the efficiency of the solar panel can be found by considering the fraction of energy lost during this time. Using a computer simulation, and increasing the total solar radiation spectrum throughout the day, an indication to the necessity of an additional night return mechanism can be appreciated.

Figure 14: Graph showing the increased gain of a solar tracker with a night return mechanism

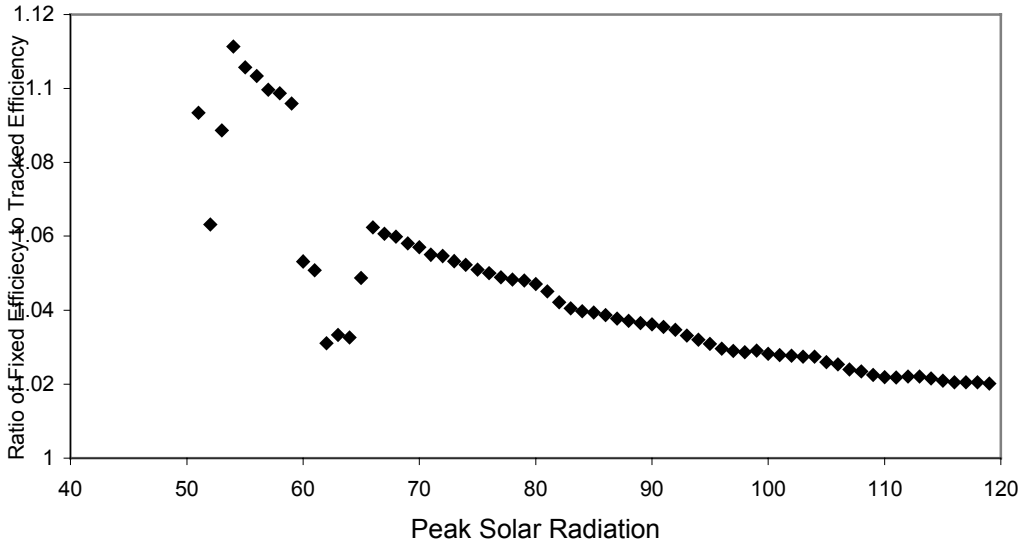

By considering the values of peak solar radiation sufficient to avoid variable efficiency responses, Figure 14 shows that for increasing levels of solar radiation, the efficiency gain provided by a night return mechanism reduces to as much as only 2% extra gain. This bears significantly on further design considerations, as the type of geographical location considered has been that of areas subjected to intense solar radiation, indicating efficiencies will be marginal at best.

Although the remainder of testing was conducted qualitatively due to insufficient equipment, the level of agreement of both the bimetallic strip and 'early morning' response testing was sufficient proof to assume the theory, and hence the computer model, was accurate.

Further manipulation of variables such as damping, bimetallic strip dimensions and size of point mass have allowed efficiencies of up to 23% extra to that of fixed panels.

10. Suggested Improvements for Enhanced Tracking Efficiency

Although tests displayed a considerable increase in solar panel efficiency throughout the average day, the system is capable of improvement. Some of the following suggestions allow for future development:

10.1 Night Return Mechanism

As described in section 9.2, the early morning response of the system, no matter how good, is finite and hence is a feature that, if changed, will immediately improve efficiency of the solar panel (although more so in areas subjected to lower amounts of solar radiation).
As an additional feature, it should perform its duty after dusk and before dawn affecting the overall workings of the solar tracker throughout the day as little as possible.
One feasible solution is to use a third bimetallic strip (of the same or similar materials) to act as a return system. This would work on the basis that the nights would bring on a considerable temperature drop, possibly to subzero temperatures. The drop in temperatures would lead to a differential rate of thermal contraction and again produce bending. This activation could then be utilised to produce a torque to return the system to its eastern starting point. Figure 15 illustrates one possible method of utilising the bending moment into a return system using a tensile wire.

Figure 15: Illustration of designed night return mechanism

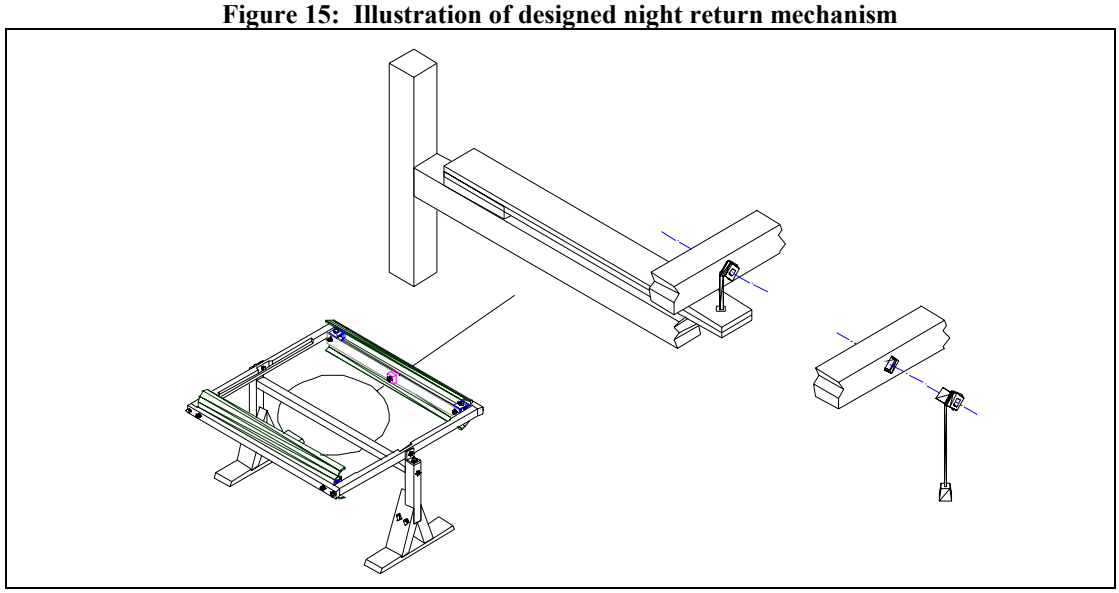

10.2 Manually Tilted Axis

Although the original concept was designed for geographic locations with 10-20^{o} of the equator, this should not constrict to that region. Providing a sufficient level of solar radiation strikes the area, this concept will function in many geographic locations, many of which are greater than 20^{o} from the equator. For example some locations may include Australasian countries, USA or Mediterranean countries.
However, using the current solar tracker design would not be the most efficient set up for a solar panel. The option of a non-horizontal axis of rotation would allow the user to control the tilt of the solar panel, compensating for the sun's zenith angle at increased latitudes. Even deciding on tilt angle is not a complicated

procedure – an inclination close to the latitude of the site will maximise the efficiency of the panel throughout the year[14]. This increase in efficiency in areas remote from the equator allows considerable scope for the development of an improved tracker and certainly merits further investigation.

10.3 Dual Axis System

The next logical improvement from the tilted axis solar tracker is to use a dual axis system. However, increasing the number of dimensions in which the solar panel can be moved is a bold venture. Not only must a second set of bimetallic strips be designed but also a second degree of damping must accompany them. Although the instigation for movement about the two different axes works on the same principle, the restraints on each are considerably different. Reorientation for the change in solar azimuth must be much more responsive, than reorientation to compensate for the changing solar altitude. Other problems also generally arise with the increased complexity of a system such as higher maintenance requirements and the increased probability of breakdown.

In terms of increased solar panel efficiency, the dual axis system, in theory, provides the greatest increase in efficiency at any location and at any time throughout the year. Although, the gains are more acute further from the equator, in most geographic regions it is not sufficient to outweigh the associated costs. If a location is found that requires the adjustment of tilt from a horizontal orientation, manual adjustment is a satisfactory compromise between increased efficiency and tracker complexity. Providing the tilted axis system is accurately directed between the summer and winter solstices (or better still, readjusted for seasonal changes) the gains will comparable to a dual axes system.

10.4 Cooling system

As well as the list of advantages photovoltaic solar panels boast, they also display one important paradox – their efficiency falls as their temperature increases. Robinson[12] stated that the maximum power output decreases with increasing temperature at approximately 0.02 mW/deg.

Although an inclusion to provide cooling to the solar panel is not specifically solving the solar tracking problem, it does have a long-term effect increasing solar panel efficiency. Designers may attempt to solve two problems at once – simultaneously cooling a photovoltaic solar panel, whilst transferring heat to cool water to supply a central heating system. Valid as this improvement would be, it would obviously have the largest effect in areas of intense solar radiation, where the thermal increases in solar panel would be significant.

11.Conclusions

It can be seen that the benefits of tracking the sun are substantial. The designed solar tracker has the potential to increase solar panel efficiency by up to 23%. This design meets its criteria by adopting a passive method of control - not draining power from the actual solar cell for movement. Although solar radiation may be insufficient in certain geographic locations, an adapted tilted/dual axis system provides accurate tracking in many locations other than those at the equator. Both the materials used and the manufacturing processes employed are available in the developing world, allowing this product to be used, replicated and maintained in many areas throughout the world.

Appendix 1: Proof for lumped mass approximation of bimetallic strip.

To determine the accuracy of assuming a bimetallic strip can be modelled as a lumped mass, the Fourier number, F_o, is used. The Fourier number compares a characteristic body dimension with an approximate temperature wave penetration depth over a given time.

$$F_o = \frac{\alpha\tau}{L^2} \qquad \text{Equation 38}$$

Where

τ	=	Time (sec)
L	=	Thickness of material (m)
α	=	Constant (m^2/s)
	=	$\frac{Thermal.Diffusivity}{Density \times Heat.Capacity} = \frac{k}{\rho c}$ Equation 39

If $F_o > 1$, the temperature has penetrated the object of thickness, L, in a time, τ, and it is suitable to model it as a lumped mass[15].
Hence the time taken for the external heat source to penetrate the body is given by

For the aluminium bar in the bimetallic strip, of thickness, 0.8mm, this criteria is satisfied after a time of 0.009 secs, and is suitable for lumped mass modelling.

Appendix 2: Computer Model of Solar Tracker

```
/*C program modelling solar tracker operation*/
/*Darren Eastwood*/
/*16th March 2003*/

#include <stdio.h>
#include <math.h>

/*Bimetallic strip dimension variables*/
float len[2][2], dl[2][2], rad[2][2],vol[2][2], area[2][2];
float hei[2], thk[2], den[2];

/*Bending dimension variables*/
float ang[2], h[2], neutral[2], dist_neutral[2];

/*Temperature variables*/
float net_Q[2][2], solrad[2], lossrad[2][2], lossconv[2][2];
float dt1[2][2],tempstep[2][2], dt[2][2];

/*Force variables*/
float apptorque[2], I_tot[2], EI[2], I[2][2];
float ymax[2], ymaxnew[2], change[2];

/*Moment variables*/
float moment[2][51], mom_wei[2][51], mom_pnt[2][51], tot_moment[2][51], x[2][51], y[2][51];
float net_torque;

/*Constants*/
float expt[2], stiff[2], alplt[2];
float blk_len, blk_hei, blk_wid, blk_vol, blk_den;
float orig_len, steps, delx;
float alps, sig, cp, peak, random, damp, s;
float pi, g, time, dtm, tinf;
float phi, theta, oldtheta, ang_vel, old_ang_vel, ang_acc, old_ang_acc;
float inertia, tot_mass, mhu, fricton;
float tot_sun_power, tot_track_power, tot_max_power;
float sun_power, track_power, max_power;
float efficiency, optimum, percentage, kn;
int i, j, k, r;

int main()
{
      /*Inputs time step*/
      printf("Input Time Step: ");
      scanf("%f", &dtm);

      /*Opening excel file*/
      FILE*ofp;
      ofp=fopen("c:Combination.xls", "w");

      /*General constants*/
      damp              =     3.6;
      kn                =     202;
      sig               =     5.669*pow(10,-8);
      cp                =     896;
      inertia           =     10;
      tot_mass          =     10;
      mhu               =     0.05;
      pi                =     M_PI;
      g                 =     9.81;
```

```
//Initial value conditions
fricton          =    g*tot_mass*mhu*(22/2)*pow(10,-3);
time             =    0;
tot_sun_power    =    0;
tot_track_power  =    0;
tot_max_power    =    0;
steps            =    50;

//Sun angle
phi              =    (5*pi/180);
//Tracker angle
theta            =    (5*pi/6);
//Tracker angular velocity
ang_vel          =    0;
//Tracker angular acceleration
ang_acc          =    0;
//Ambient temperature
tinf             =    19.2*sin(phi)+ 278.9;

//Block dimensions and constants
blk_len          =    40*pow(10,-3);
blk_hei          =    80*pow(10,-3);
blk_wid          =    17*pow(10,-3);
blk_vol          =    blk_len*blk_hei*blk_wid;
blk_den          =    7800;

//Material densities
den[0]           =    2700;
den[1]           =    7800;

//Original material dimensions
hei[0]           =    50*pow(10,-3);
thk[0]           =    0.8*pow(10,-3);
hei[1]           =    50*pow(10,-3);
thk[1]           =    0.8*pow(10,-3);

len[0][0]        =    830*pow(10,-3);
len[0][1]        =    830*pow(10,-3);
len[1][0]        =    830*pow(10,-3);
len[1][1]        =    830*pow(10,-3);
orig_len         =    len[0][0];
delx             =    orig_len/steps;

//Coefficients of themal expansion
expt[0]          =    24*pow(10,-6);
expt[1]          =    11*pow(10,-6);
//Material stiffnesses
stiff[0]         =    70*pow(10,9);
stiff[1]         =    210*pow(10,9);
//Material absorbivity values
alplt[0]         =    0.95;
alplt[1]         =    0.04;
alps             =    0.96;

//Calculating area and volume dimensions
//and defining initial conditions

for(j=0;j<=1;j++)
{
    for(i=0;i<=1;i++)
    {
        area[i][j]       =    len[i][j]*hei[i];
```

```
                vol[i][j]       =       len[i][j]*hei[i]*thk[i];

                dt1[i][j]       =       tinf;
                apptorque[j]    =       0;
        }
}

//Initialising bimetallic strip shape

for(j=0;j<=1;j++)
{
        for(k=0;k<51;k++)
        {
                y[j][k]  =      0;
                x[j][k]  =      delx*k;
        }
}

do
{
    //Resets initial conditions
    for(i=0;i<=1;i++)
    {
                for(j=0;j<=1;j++)
                {
                        len[i][j]       =       830*pow(10,-3);
                        ymaxnew[j]      =       0;
                        ymax[j]         =       0;
                }
                h[i]    =       10;
    }
//Solar radiation and ambient temperature variation
//over the course of a day.
peak            =       1200*sin(phi);
tinf            =       19.2*sin(phi)+ 278.9;

//Outputs
if(time==(2*r))
{
        fprintf(ofp,"%f,%f,%f\n", time,phi,theta);
        printf("Time = %f\t", time);
        printf("Theta = %f\t", theta);
        printf("Phi = %f\t", phi);
        r       = r+1;
}
    //Heating of bimetallic strips dicated by tracker orientation
    if((phi-theta)>0)
                {
                solrad[0]       =       sin(phi-theta)*peak*alps;
                solrad[1]       =       0;
                }
    else if((phi-theta)<0)
                {
                solrad[0]       =       0;
                solrad[1]       =       sin(theta-phi)*peak*alps;
                }
      else
               {
                solrad[0]       =       0;
                solrad[1]       =       0;
                }
```

```
for(i=0;i<=1;i++)
{
        for(j=0;j<=1;j++)
        {
                //Thermal interactions of the bar with its surroundings
                lossrad[i][j]       =       alplt[i]*sig*(pow(dt1[i][j],4)-pow(tinf,4));
                lossconv[i][j]      =       2*h[i]*(dt1[i][j]-tinf);
                net_Q[i][j]         =       solrad[j] - (lossrad[i][j]+lossconv[i][j]);
                tempstep[i][j]      =       (net_Q[i][j]*area[i][j]*dtm)/(den[i]*vol[i][j]*cp);

                //Resulting Temperature Changes
                dt1[i][j]           =       dt1[i][j]+tempstep[i][j];
                dt[i][j]            =       dt1[i][j]-tinf;

                //Entensions in Length
                dl[i][j]    =       len[i][j]*expt[i]*dt[i][j];
        }
}
        //Finds radius of curvature for both bimetallic strips
        for(j=0;j<=1;j++)
        {
                //Allows for the case infinite radius of curvature

                if(((dl[0][j]==0)&&(dl[1][j]==0))||(dl[0][j]==dl[1][j]))
                {
                        for(k=0;k<=50;k++)
                        {
                                moment[j][k]    =       0;
                        }

                dist_neutral[j] = ((0.5*stiff[0]*hei[0]*pow(thk[0],2))-
                stiff[1]*thk[1]*hei[1]*(thk[0]+0.5*(thk[1])))/(stiff[0]*(thk[0]*hei[0])-
                stiff[1]*(thk[1]*hei[1]));

                //Second moment of area
                I[0][j]    =(hei[0]*pow(thk[0],3)/12)+hei[0]*thk[0]*pow((thk[0]-
                dist_neutral[j]),2);
                I[1][j]    =(hei[1]*pow(thk[1],3)/12)+hei[1]*thk[1]*pow((thk[0]+thk[1]-
                dist_neutral[j]),2);

                //Total rigidity and second moment of area
               I_tot[j]   =I[0][j]+I[1][j];
               EI[j]      =(I[0][j]*stiff[0])+(I[1][j]*stiff[1]);
                }

                //Finds radius of curvature and hence applied moment
               else
                {
                rad[1][j]           =
                ((len[1][j]+dl[1][j])*(0.5*(thk[0]+thk[1])))/(dl[0][j]-dl[1][j]);
                rad[0][j]           =       rad[1][j]+0.5*(thk[0]+thk[1]);

                //Angle of curve (Radians)
                ang[j]    =       (len[0][j]+dl[0][j])/rad[0][j];

               //Neutral axis
               neutral[j]=       orig_len/ang[j];

                //Second moment of area
                 I[0][j]    =       (hei[0]*pow(thk[0],3)/12)+hei[0]*thk[0]*pow((rad[0][j]-
                neutral[j]),2);
```

```
                I[1][j]    =          (hei[1]*pow(thk[1],3)/12)+hei[1]*thk[1]*pow((rad[1][j]-
                neutral[j]),2);

                //Total rigidity and second moment of area
                I_tot[j]    =          I[0][j]+I[1][j];
                EI[j]       =          (I[0][j]*stiff[0])+(I[1][j]*stiff[1]);

                for(k=0;k<=50;k++)
                {
                        //Moment due to heating
                        moment[j][k]    =          EI[j]/(0.5*(rad[0][j]+rad[1][j]));
                }

                }
}

//Finds moment values along the length of each bimetallic strip
for(k=0;k<=50;k++)
{
        if(x[0][k]<orig_len/2)
        {
                //Moment due to self weight unit force (before midpoint)
                mom_wei[0][k]
                =0.25*pow((x[0][k]),2)*(cos(theta)*(g*((vol[0][j]*den[0])+(vol[1]
                [j]*den[1]))/orig_len));

                //Moment of point mass(before midpoint)
                mom_pnt[0][k] =0.25*(x[0][k])*cos(theta)*g*blk_vol*blk_den;
        }

else
        {
                //Moment due to self weight unit force (after midpoint)
                mom_wei[0][k] =0.25*pow((orig_len-
                (x[0][k])),2)*(cos(theta)*(g*((vol[0][j]*den[0])+(vol[1][j]*den[1]))
                /orig_len));

                //Moment of point mass (after midpoint)
                mom_pnt[0][k] =0.25*(orig_len-
                (x[0][k]))*cos(theta)*g*blk_vol*blk_den;
        }

tot_moment[0][k]    =      moment[0][k]-mom_wei[0][k]-mom_pnt[0][k];

                if(x[1][k]<orig_len/2)
        {
        //Moment due to self weight unit force (before midpoint)
         mom_wei[1][k]
         =0.25*pow((x[0][k]),2)*(cos(theta)*(g*((vol[0][j]*den[0])+(vol[1][j]*den[1
         ]))/orig_len));

        //Moment of point mass(before midpoint)
        mom_pnt[1][k] =0.25*(x[0][k])*cos(theta)*g*blk_vol*blk_den;
        }

         else
        {
        //Moment due to self weight unit force (after midpoint)
         mom_wei[1][k] =0.25*pow((orig_len-
         (x[1][k])),2)*(cos(theta)*(g*((vol[0][j]*den[0])+(vol[1][j]*den[1]))/orig_le
         n));
```

```
                    //Moment of point mass (after midpoint)
                     mom_pnt[1][k] =0.25*(orig_len-
                     (x[1][k]))*cos(theta)*g*blk_vol*blk_den;
                    }

                     tot_moment[1][k]    =
                     moment[1][k]+mom_wei[1][k]+mom_pnt[1][k];

          }


          //Cycles for both bimetallic strips
          for(j=0;j<=1;j++)
          {
                    do
                      {
                                //Cycles for incremental steps along the bar
                                for(k=1;k<=49;k++)
                                {
                                //End conditions
                                y[j][0]=0;
                                y[j][51]=0;

                                //Displacement for Bar 'j' at a distance 'k' along it

                                y[j][k]=0.5*((tot_moment[j][k]/EI[j])*(pow(delx,2))+y[j][
                                k+1]+y[j][k-1]);

                                //Cycles to find the maximum displacement
                                if(fabs(y[j][k])>fabs(y[j][k-1]))
                                {
                                     ymaxnew[j]=y[j][k];
                                }
                           }
                           change[j]=fabs((ymaxnew[j]-ymax[j]));
                           ymax[j]=ymaxnew[j];

                          //Imposes accuracy limit
                      }while(change[j]>0.001);
          }

//Updating total Length of Bimetallic strips
for(i=0;i<=1;i++)
{
          len[i][j] =    len[i][j]+dl[i][j];
}

for(j=0;j<=1;j++)
{
          apptorque[j]      =       blk_vol*blk_den*g*ymax[j];
          fricton           =       g*tot_mass*mhu*(22/2)*pow(10,-3);
}

//Net torque calculations
if(fabs(apptorque[0]-apptorque[1])>fricton)
{
          if(apptorque[0]>apptorque[1])
          {
                    net_torque=(apptorque[0]-apptorque[1]-fricton)-(inertia*ang_acc)-
                    (damp*ang_vel);
          }
          else
```

```
		{
			net_torque=-1*(apptorque[1]-apptorque[0]-fricton)-(inertia*ang_acc)-
			(damp*ang_vel);
		}
	}
	else
	{
		if(apptorque[0]>apptorque[1])
		{
			net_torque	=(apptorque[0]-apptorque[1]-fricton)-
			(inertia*ang_acc)-(damp*ang_vel);
			if(net_torque<0)
			{
				net_torque=0;
			}
		}
		else
		{
			net_torque	=	-1*(apptorque[1]-apptorque[0]-fricton)-
			(inertia*ang_acc)-(damp*ang_vel);
			if(net_torque>0)
			{
				net_torque=0;
			}
		}
	}

	//Integrating over time steps to find solar tracker orientation
	old_ang_acc	=	ang_acc;
	ang_acc		=	net_torque/inertia;
	old_ang_vel	=	ang_vel;
	ang_vel		=	old_ang_vel+0.5*(ang_acc+old_ang_acc)*dtm;
	oldtheta	=	theta;
	theta		=	oldtheta +
	0.5*((ang_vel+old_ang_vel)*dtm)+0.5*((ang_acc+old_ang_acc)*pow(dtm,2));

	 //Imposing end conditions on solar tracker movement
	 if(theta<(pi/6))
	{
			theta	=	pi/6;
	}
	 else if(theta>(5*pi/6))
	{
			theta	=	5*pi/6;
	}

	 //Calculating incremental power obtained
	 max_power		=	peak;
	 sun_power		=	peak*sin(phi);
	 if(fabs(theta-phi)<pi/4)
	 {
			track_power	= peak*cos(fabs(phi-theta));
	 }
	 else
	 {
			track_power	= 0;
	 }

	 //Calculating total power obtained
	tot_max_power	=	tot_max_power + max_power;
	tot_sun_power	=	tot_sun_power + sun_power;
	tot_track_power	=	tot_track_power + track_power;
```

```
        time                    =       time+dtm;
        phi                     =       phi+(pi*dtm/43200);
        }while(phi<(175*pi/180));

        //Calculating Efficiencies
        efficiency              =       tot_track_power/tot_sun_power;
        optimum                 =       tot_max_power/tot_sun_power;
        percentage              =       efficiency/optimum;

        //Efficiency Outputs
        printf("efficiency = %f\t", efficiency);
        printf("Optimum = %f\n", optimum);

        fclose (ofp);
        return 0;
}
```

Acknowledgements

For helping me make the progress I've made, I feel it necessary to thank the following people:

- Dr. S. Pickering – For his advice and consultation on bimetallic strip thermodynamics.
- Dr. I Care – For helping me to take a novel outlook and for providing essential advice at the conceptual stages.
- Dr. R. Wilson – For his help throughout the design and for organising testing facilities.
- Dr. M. J. Clifford – For his constant support, guidance and encouragement throughout the year.

References

[1] Cheremisinoff, P.N; Regino, T.C, (1978); "*Principles & Applications of Solar Energy"*, Ann Arbor Science, Page 81.

[2] www.e-marine-inc.com, accessed 30/10/2002.

[3] Poulek, V.; Libra, M.; (1998) *"New Solar Tracker: Solar Energy Materials and Solar Cells"*, Vol.51, Issue 2.

[4] Zomeworks Passive Energy Products, www.zomeworks.com/solar/trackrack/trackrack.html, accessed 22/11/2002.

[5] Taos Green Solar, Mark Coleman, www.southwestsolar.com/side_by_side.htm; accessed 02/12/2002

[6] Greenhouses Del Sol, www.greenhousesandsunrooms.com, accessed 28/11/2002.

[7] TiNi Aerospace, Inc., www.tiniaerospace.com, accessed 05/11/2002.

[8] Gere, J.M; (2001), *"Mechanics of Materials"*, Brooks/Cole, Page 23.

[9] Holman, J.P.; (1997), *"Heat Transfer (8th Edition)"*, McGraw-Hill, Page 479.

[10] Tipler, P, A; (1999), *"Physics for Scientists and Engineers (4th Edition)"*, Freeman Worth, Page 634.

[11] Wieder, S.; (1982), *"An Introduction to Solar Energy for Scientists and Engineers"*, John Wiley & sons, Page 35.

[12] Robinson, N.; (1964), "*Solar Radiation*", Elsevier Publishing Company.

[13] White, F., M.;(1999), *"Fluid Mechanics (Fourth Edition)"*, McGraw-Hill, Page 458.

[14] Markvart, T (Editor); (1994), *"Solar Electricity"*, John Wiley & Sons, Page 19.

[15] Rodgers, G; Mayhew, Y; (1992), *"Engineering Thermodynamics: Work and Heat Transfer (4th Edition)"*, Prentice Hall, Page 525.